ISSN 1674-1056
http://cpb.iphy.ac.cn
http://iopscience.iop.org/cpb
中国物理 B
Chinese Physics
中国物理
Chinese Physics B

A novel receiver-transmitter metasurface for a high-aperture-efficiency Fabry-Perot resonator antenna

Peng Xie(谢鹏), Guangming Wang(王光明), Binfeng Zong(宗彬锋), and Xiaojun Zou(邹晓鋆)
Citation: Chin. Phys. B, 2021, 30 (**8**): 084103. DOI: 10.1088/1674-1056/ac0788
Journal homepage: http://cpb.iphy.ac.cn; http://iopscience.iop.org/cpb

What follows is a list of articles you may be interested in

Shared aperture metasurface antenna for electromagnetic vortices generation with different topological charges

He Wang(王贺), Yong-Feng Li(李勇峰), and Shao-Bo Qu(屈绍波)
Chin. Phys. B, 2021, 30 (**8**): 084101. DOI: 10.1088/1674-1056/abe37c

Ultra-thin single-layer transparent geometrical phase gradient metasurface and its application to high-gain circularly-polarized lens antenna

Tang-Jing Li(李唐景), Jian-Gang Liang(梁建刚), Hai-Peng Li(李海鹏), Ya-Qiao Liu(刘亚峤)
Chin. Phys. B, 2016, 25 (**9**): 094101. DOI: 10.1088/1674-1056/25/9/094101

Optimization of loss and gain multilayers for reducing the scattering of a perfect conducting cylinder

Zhen-Zhong Yu(余振中), Guo-Shu Zhao(赵国树), Gang Sun(孙罡), Hai-Fei Si(司海飞), Zhong Yang(杨忠)
Chin. Phys. B, 2016, 25 (**7**): 074101. DOI: 10.1088/1674-1056/25/7/074101

Design of ultra wideband microwave absorber effectual for objects of arbitrary shape

Gong Yuan-Xun, Zhou Zhong-Xiang, Jiang Jian-Tang, Zhao Hong-Jie
Chin. Phys. B, 2015, 24 (**12**): 124101. DOI: 10.1088/1674-1056/24/12/124101

Bidirectional reflectance distribution function modeling of one-dimensional rough surface in the microwave band

Guo Li-Xin, Gou Xue-Yin, Zhang Lian-Bo
Chin. Phys. B, 2014, 23 (**11**): 114102. DOI: 10.1088/1674-1056/23/11/114102

A novel receiver–transmitter metasurface for a high-aperture-efficiency Fabry–Perot resonator antenna*

Peng Xie(谢鹏), Guangming Wang(王光明)†, Binfeng Zong(宗彬锋), and Xiaojun Zou(邹晓鋆)

Air and Missile Defense College, Air Force Engineering University, Xi'an 710051, *China*

(Received 20 February 2021; revised manuscript received 7 April 2021; accepted manuscript online 3 June 2021)

This paper presents a novel coupled receiver–transmitter metasurface (MS) which is used to realize a high-aperture-efficiency Fabry–Perot resonator antenna. The unit cell of the MS adopts a slot-coupling procedure to realize energy transmission from the receiver patch to the radiator patch. This approach makes it easier to independently control the transmission magnitude and phase. Based on this characteristic, the transmission coefficients of different unit cells on the MS can be optimized by a genetic algorithm. Then, nearly uniform electric amplitude and phase distribution across the aperture field of the antenna are achieved. Therefore, the gain and aperture efficiency of the antenna are improved. A prototype of the optimized antenna is fabricated and measured to validate the design. The measured gain of the fabricated antenna reaches 17.3 dBi with an aperture efficiency of 94.5%. A higher aperture efficiency is obtained with the proposed antenna which has a low profile and simple structure.

Keywords: receiver–transmitter metasurface, transmission coefficients manipulation, genetic algorithm, high aperture efficiency, Fabry–Perot resonator antenna

PACS: 41.20.Jb, 73.20.Mf **DOI:** 10.1088/1674-1056/ac0788

1. Introduction

High-efficiency antennas with a simple structure are urgently required in many wireless communication systems because they can provide high directivity with a small aperture size.[1,2] Fabry–Perot (FP) resonator antennas have received continuous attention since their proposal due to their inherent high gain characteristic.[3,4] They usually consist of a ground plane, a partially reflective surface (PRS) and a radiator in the cavity. In this paper, we replace the PRS with a well-designed metasurface (MS). The electromagnetic waves resonate in the cavity and leak out of the cavity from the MS. When the electromagnetic waves coming out of the MS are in phase, the antenna can realize high-gain radiation in the far field. The resonant condition of the antenna can be expressed as[5]

$$\varphi_{\mathrm{MS}} + \varphi_{\mathrm{G}} - \frac{4\pi h}{\lambda_0} = 2N\pi, \quad N = 0, 1, 2, \ldots, \tag{1}$$

where φ_{MS} and φ_{G} represent the reflection phase of the MS and the ground plane, respectively. h is the distance between the MS and the ground plane and λ_0 is the wavelength in free space. From this equation, it is apparent that the height of the cavity is closely related to the reflection phase of the MS. On the other hand, the reflection magnitude of the MS, R, determines the directivity, D, of the FP antenna. The relationship between R and D can be summarized as[6]

$$D_{\mathrm{r}} = 10\log\frac{1+R}{1-R}, \tag{2}$$

where D_{r} is the directivity enhancement of the resonator antenna relative to the radiator. It can be seen that D_{r} increases with increase in R. For the purpose of enhancing the aperture efficiency of the resonator antenna, the antenna must have high directivity. Thus, the MS needs be highly reflective.

There are many reports on high-gain and high-efficiency FP resonator antennas.[7–9] According to the theoretical analysis of FP resonator antennas, the electromagnetic waves coming out from the cavity have the same phase. However, in practice, the antenna often presents a non-uniform electric field amplitude and phase distribution across the aperture field, which can affect the gain of the antenna to some extent. Therefore, near-field correction is an effective way to further enhance the gain of the antenna.[10–14] A double-side printed dielectric with non-uniform reflection magnitude and phase was chosen as the superstrate of the FP resonator antenna in Ref. [10]. The measured maximum gain of the antenna was 15.75 dBi with an aperture efficiency of 61.8%. In Refs. [11,12], all-dielectric near-field correcting structures (NFCS) were designed to correct the near-field distribution of the antenna to enhance the gain of the antenna. A double-layer non-uniform superstrate (DNS) was designed and optimized to improve the aperture efficiency of the FP resonator antenna in Ref. [13]. The directivity of the antenna was improved to 20.4 dBi with an aperture efficiency of 91.7%. However, a NFCS or DNS both increase the profiles of the antennas and make them complex. A simple device that can correct both the amplitude and the phase of the electric field simultaneously is imperative to overcome these drawbacks.

In this paper, a coupled receiver–transmitter MS is de-

*Project supported by the National Natural Science Foundation of China (Grant No. 61871394) and Natural Science Foundation of Shanxi Province, China (Grant No. 2020JQ-482).

†Corresponding author. E-mail: wgming01@sina.com

© 2021 Chinese Physical Society and IOP Publishing Ltd

signed to realize high aperture efficiency of a FP resonator antenna. The unit cell of the MS adopts a coupling slot to realize wave transmission from the receiver patch to the radiator patch. This is conducive to the control of the unit cell characteristics. Then, the transmission magnitudes and phases of different unit cells on the MS are optimized by a genetic algorithm (GA)[15,16] to further enhance the gain and efficiency, in which case the electric amplitude and phase across the aperture field of the antenna are corrected to a nearly uniform distribution. Finally, the gain of the antenna reaches 17.3 dBi with an aperture efficiency of 94.5%.

2. Design of the receiver–transmitter unit cell

A coupled receiver–transmitter unit cell is adopted when designing a MS that is suitable for a FP resonator antenna. The construction of the unit cell is displayed in Fig. 1. The unit cell consists of two substrates and a three-layer metal structure. The substrates are of the F4B type with a thickness of 1.6 mm ($t_1 = t_2 = 1.6$ mm) and a relative permittivity of 2.65. The top and bottom layers of the unit cell are square patches of the same size, while the middle layer of the unit cell is an all-metal plane with a rectangular slot at the center. The two patches operate as receiver and radiator, respectively. The rectangular slot in the middle layer is used to realize coupling between the two patches. The operating principle of the unit cell is similar to the receiving and radiation mechanisms of two slot-coupled patch antennas. The incident wave is received by the receiver patch and coupled to the radiator patch through the slot in the middle layer. The period of the unit cell p is set to 8 mm. The unit cell is simulated by the CST and the simulation model is shown in Fig. 1(b).

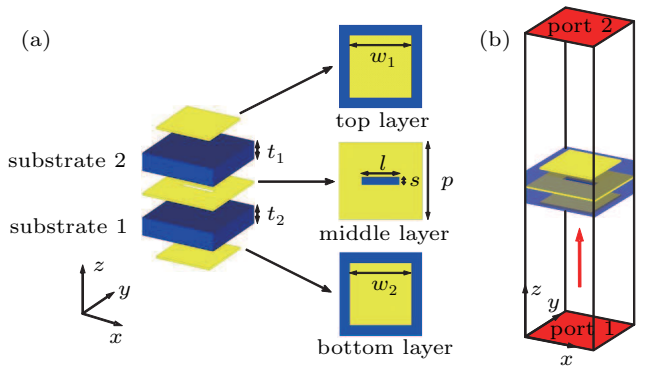


Fig. 1. Construction of the unit cell. (a) Detailed views of three layers of the unit cell. (b) Simulation model in the CST.

The operating frequency of the unit cell is determined by the size of the two patches. After simulation, the unit cell can operate at 10 GHz when $w_1 = w_2 = 6.6$ mm. The transmission magnitude of the unit cell is related to the length of the slot l. This can be understood from the aspect of impedance matching of the antenna. A decrease in l can increase the impedance of the slot and cause impedance mismatching between the slot and the two patches, thus the reflectivity of the unit cell is increased and the transmittivity is decreased. The variation of the characteristics of the unit cell with l is shown in Fig. 2.

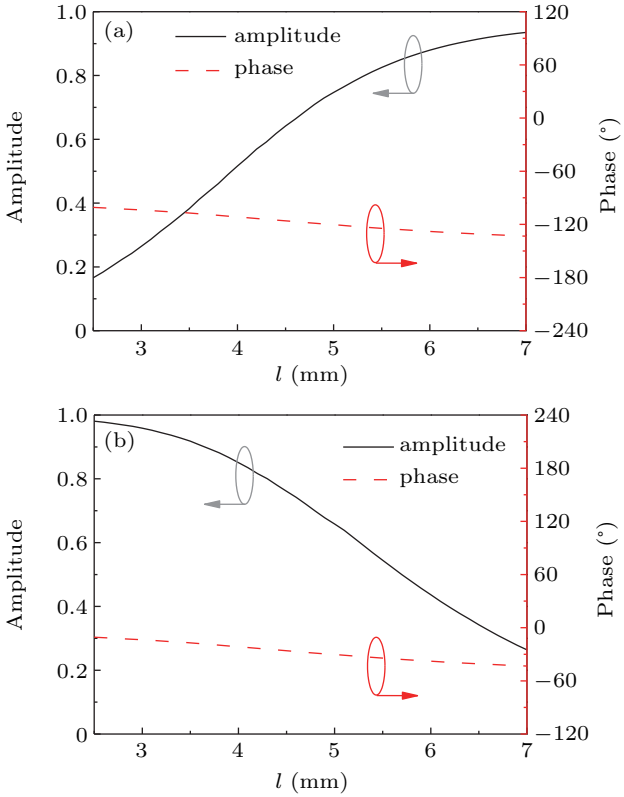


Fig. 2. Effect of l on the S parameters of the unit cell: (a) transmission coefficients, (b) reflection coefficients.

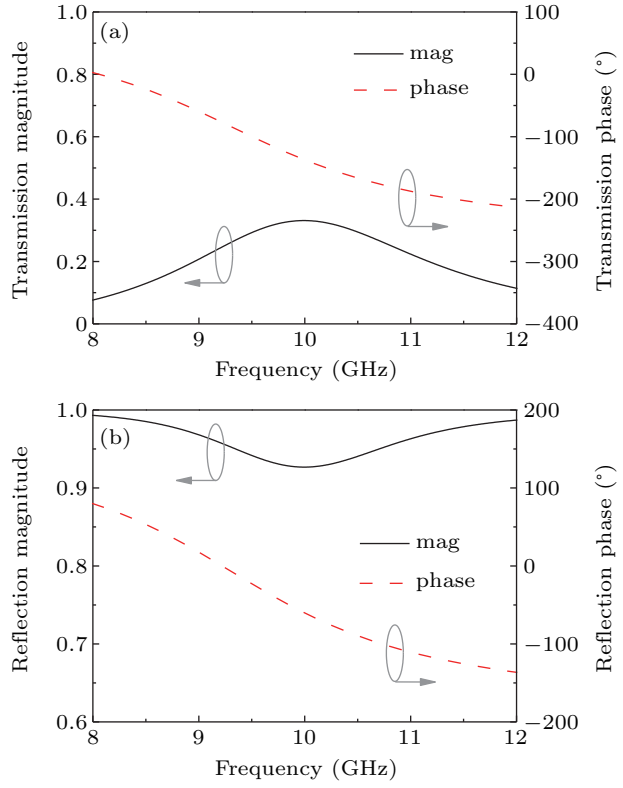


Fig. 3. The S parameters of the unit cell when $l = 3$ mm: (a) transmission coefficients, (b) reflection coefficients.

It can be seen that the transmission magnitude of the unit cell goes up from 0.18 to 0.92 as l varies from 2.5 to 7, while the reflection magnitude goes down from 0.98 to 0.22. From Eq. (2), it is known that high reflectivity of the MS can lead to high gain of the antenna. Therefore the length of the slot l is set to 3 mm to make the unit cell highly reflective. The characteristics of the unit cell with $l = 3$ mm are shown in Fig. 3. The reflection magnitude of the unit cell reaches 0.94 at 10 GHz. The reflection phase of the unit cell is $-60.2°$, which can be used to calculate the height of the cavity according to Eq. (1).

On the other hand, the transmission phase of the unit cell is affected by the size of the radiator patch. The variation of the S parameters of the unit cell with the size of transmitter patch (w_2) is presented in Fig. 4. As the width of the radiator patch w_2 increases from 4 mm to 7.9 mm, the transmission phase of the unit cell goes down from $-37°$ to $-185°$, while the reflection magnitude and phase are barely affected. This is because the larger patch size can cause a transmission phase delay of the unit cell. Therefore the transmission phase decreases with increase in the size of the transmitter patch.

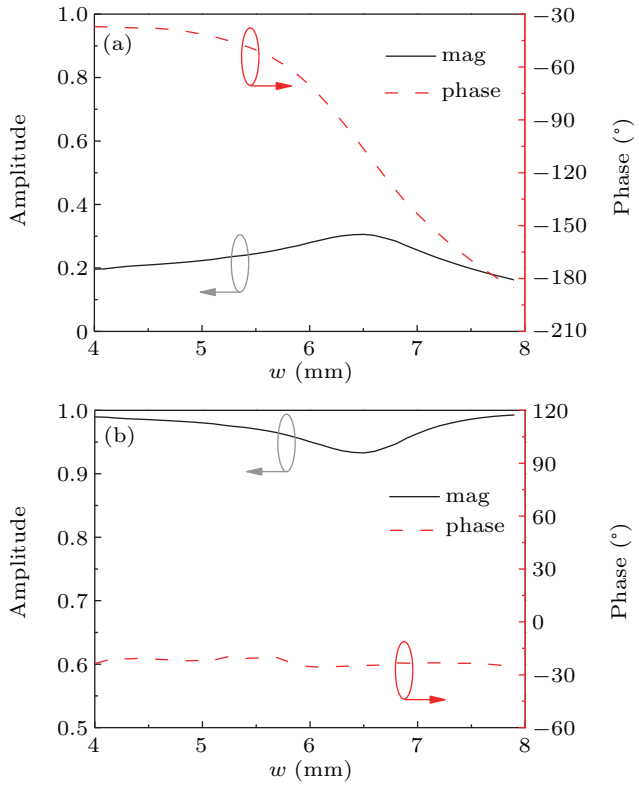


Fig. 4. Characteristics of the unit cell vary with w_2: (a) transmission coefficients, (b) reflection coefficients.

Above all, the transmission magnitude and phase of the unit cell can be tuned by the length of the slot and the width of the radiator patch, respectively. In addition, the reflection phase is not affected when l and w_2 are changed, which guarantees that the resonance condition in the cavity is not influenced when the transmission magnitude and phase of different unit cells on the MS are changed.

3. Design of a high-aperture-efficiency resonator antenna

A unit cell with $l = 3$ mm and $w_2 = 6.6$ mm is chosen as the original unit cell and a MS is formed from 9×9 unit cells. The MS is cut to a circle with a radius of 36 mm because the unit cells on the corners of the MS make little contribution to the gain of the antenna. Four unit cells around the edge of the antenna are removed and replaced by four holes to accommodate four dielectric cylinders to support the MS above the feed antenna.

A slot-coupled patch antenna is chosen as the radiator of the antenna, as shown in Fig. 5(a). The antenna also consists of two substrates and a three-layer metal structure. The materials of the two substrates are the same as the MS but with different thicknesses. The thickness of the top substrate is 1.6 mm and that of the bottom substrate is 0.8 mm. The top layer is the radiation patch and the bottom layer is the feeding line with a characteristic impedance of 50 Ω. The middle layer between the two substrates is an all-metal ground plane with a slot etched under the radiation patch. The feed antenna is also designed to be round to match with the MS and the substrates at the endpoint of the feeding line are cut flat to facilitate welding the SMA connector. Combining the feed antenna and the designed MS, antenna 1 is formed. A model of the antenna in CST is displayed in Fig. 5(b). The antenna is simulated by CST and the height of the antenna cavity is set to 4.5 mm after optimization.

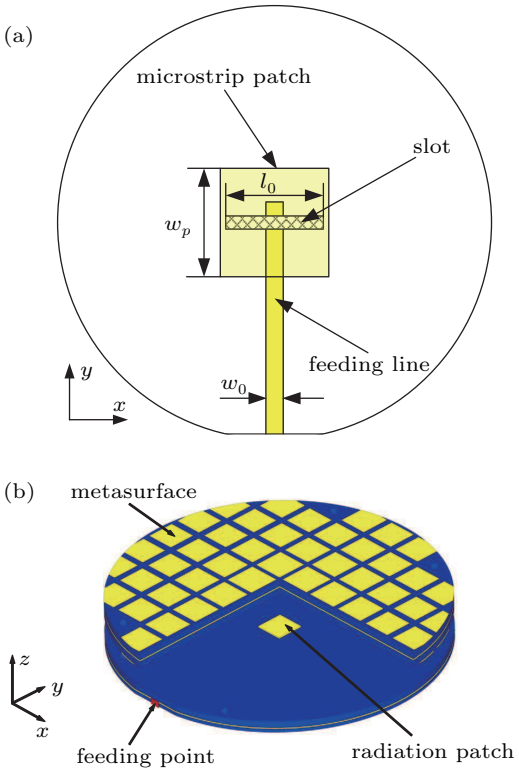


Fig. 5. (a) Schematic diagram of the feed antenna ($l_0 = 5.9$ mm, $w_p = 6.2$ mm, $w_0 = 2.16$ mm). (b) Model of the FP antenna.

According to the theoretical analysis, a resonator antenna can obtain uniform phase and amplitude distribution across the aperture field when the resonance condition in Eq. (1) is satisfied. However, the phase and amplitude on the reference plane are non-uniform. Figure 6 presents the simulated electric amplitude and phase distribution on a reference plane in the near field of antenna 1, which is set above the antenna at a distance of 20 mm. There is a huge phase and amplitude difference between the center and the edge of the antenna. In order to obtain higher gain, a uniform phase and amplitude distribution across the aperture field of the antenna is necessary. Thus, the transmission phase and magnitude of different unit cells on MS need to be carefully tuned to give the antenna a uniform phase and amplitude distribution. Thus, the GA is adopted to optimize the gain of the antenna by tuning the transmission magnitude and phase of different unit cells on the MS. The range of T_n is set as 0.16–0.93 with l varying from 2.7 to 7 mm, and the range of φ_n is set as $-37°$ to $-185°$ with w_2 varying from 4 to 7.9 mm. The unit cells on the MS are numbered as shown in Fig. 7.

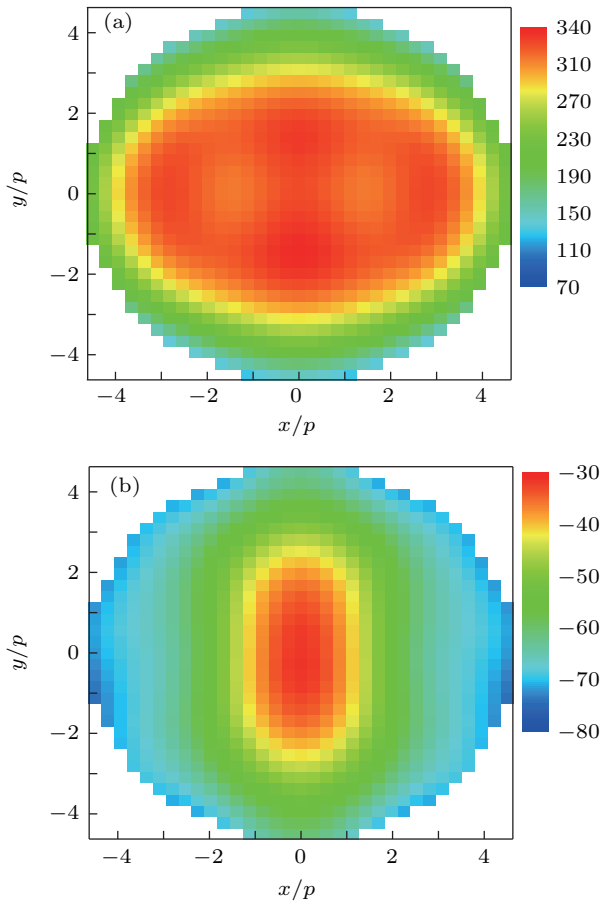


Fig. 6. The electric field distribution on the reference plane of antenna 1: (a) amplitude distribution, (b) phase distribution.

Observing that the unit cells on the MS are rotationally symmetric with respect to the center, only five unit cells, lying on the $+x$-axis, are optimized by the GA. The parameters of other unit cells are deduced by linear interpolation according to their distance from the center of the MS, which can greatly reduce the optimization time. Then the gene sequence of the algorithm can be expressed as

$$i = (T_0, \varphi_0, T_1, \varphi_1, T_2, \varphi_2, T_3, \varphi_3, T_4, \varphi_4). \tag{3}$$

In this individual, the transmission magnitudes and phases of five unit cells are arranged in sequence. Each individual represents a kind of transmission magnitude and phase distribution on the MS. The initial gene sequence is set as (0.34, $-47.2°$, 0.34, $-47.2°$, 0.34, $-47.2°$, 0.34, $-47.2°$, 0.34, $-47.2°$), which is the transmission magnitude and phase of the unit cell used in Antenna 1. The parameter values of different unit cells on the MS are determined according to Figs. 2 and 4. Then the algorithm invokes the CST to simulate the antenna with the MS determined by the individual i. After simulation, the realized gain of the antenna is returned to the algorithm. For the purpose of obtaining high aperture efficiency of the antenna, the fitness of the algorithm is set as

$$\max \eta = \frac{G\lambda_0^2}{4\pi^2 R^2}, \tag{4}$$

where G is the realized gain of the antenna and R is the radius of the MS. In the GA, the population size in per generation is set to 50. The initial population contains the initial gene sequence and other randomly generated gene sequences. The probabilities of crossover and mutation operation are 0.2 and 0.1, respectively. One hundred generations are adopted by the algorithm.

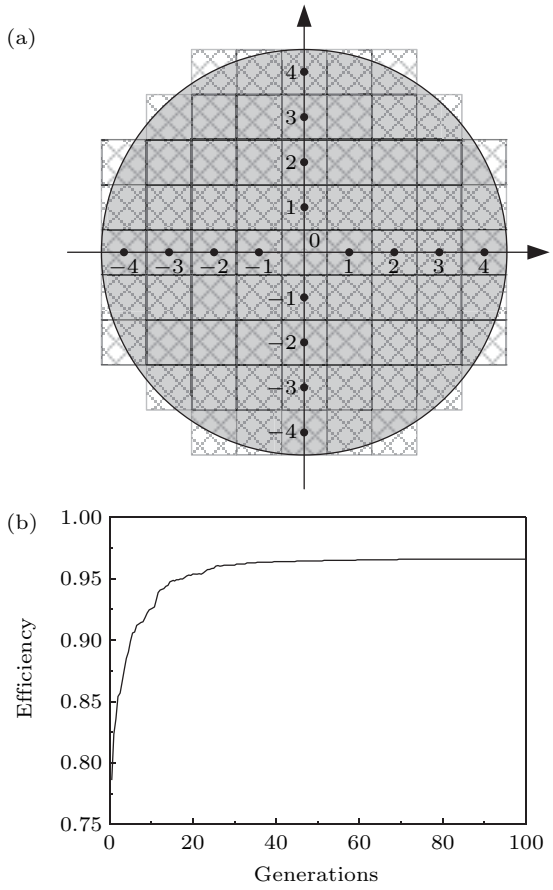


Fig. 7. (a) The numbering of unit cells on the MS and (b) the convergence curve of the optimization algorithm.

Based on the above settings, the GA is run to optimize the aperture efficiency of the antenna. The convergence of η is plotted in Fig. 7(b). After 50 generations, the aperture efficiency of the antenna trends as stable. Optimized transmission coefficients of different unit cells are finally determined and are shown in Table 1, with parameters values of the unit cells. According to the optimized results, an improved MS is arranged and the antenna formed by it is named antenna 2. Figure 8 shows the three layers of the improved MS. Other parts of antenna 2 are the same as antenna 1.

Table 1. Optimized transmission coefficients and corresponding parameters values of the unit cell.

No.	T_n	φ_n (°)	l (mm)	w_2 (mm)
0	0.31	−175.5	3.16	7.26
1	0.31	−169.8	3.18	7.12
2	0.32	−154.1	3.24	6.82
3	0.34	−137.4	3.32	6.60
4	0.41	−130.2	3.54	6.52

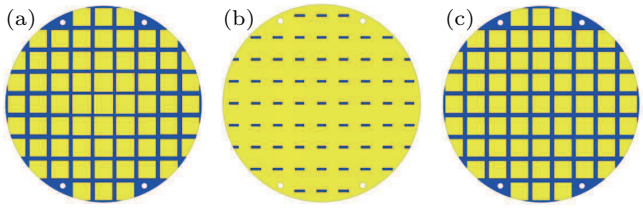


Fig. 8. Views of the improved MS: (a) top layer, (b) middle layer, (c) bottom layer.

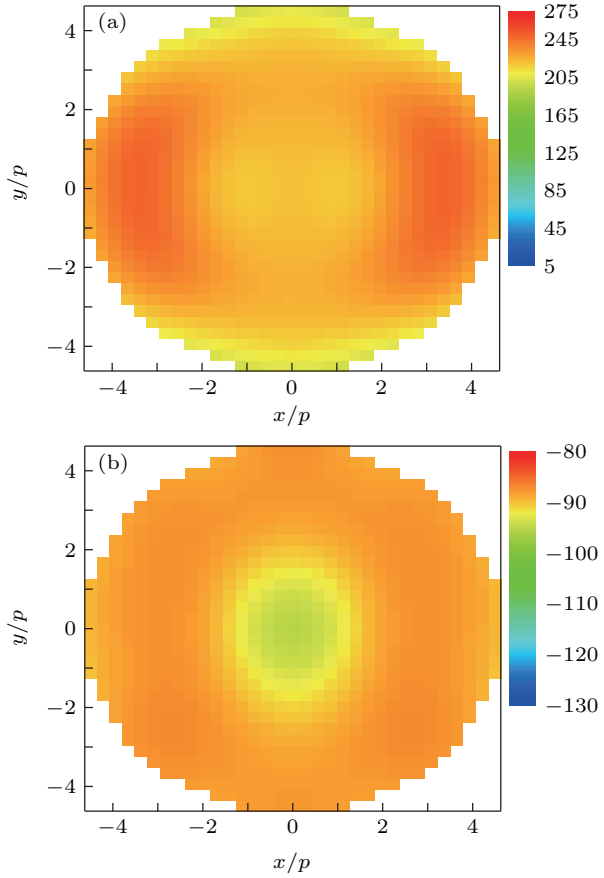


Fig. 9. Electric field distribution on the reference plane of antenna 2: (a) amplitude distribution, (b) phase distribution.

4. Simulated and measured results

To show the performance improvement of antenna 2, the near-field characteristics of the antenna are investigated. Figure 9 presents the electric field distribution on the reference plane of antenna 2. It can be seen that the antenna has a more uniform amplitude and phase distribution after optimization, which ensures the antenna can realize a higher gain, and thus higher efficiency.

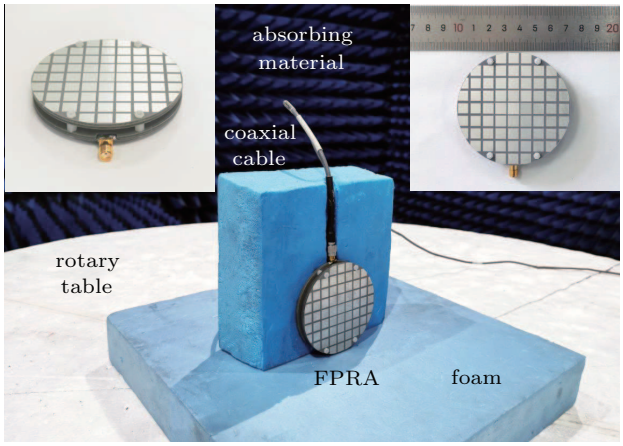


Fig. 10. The fabricated antenna and the measurement environment.

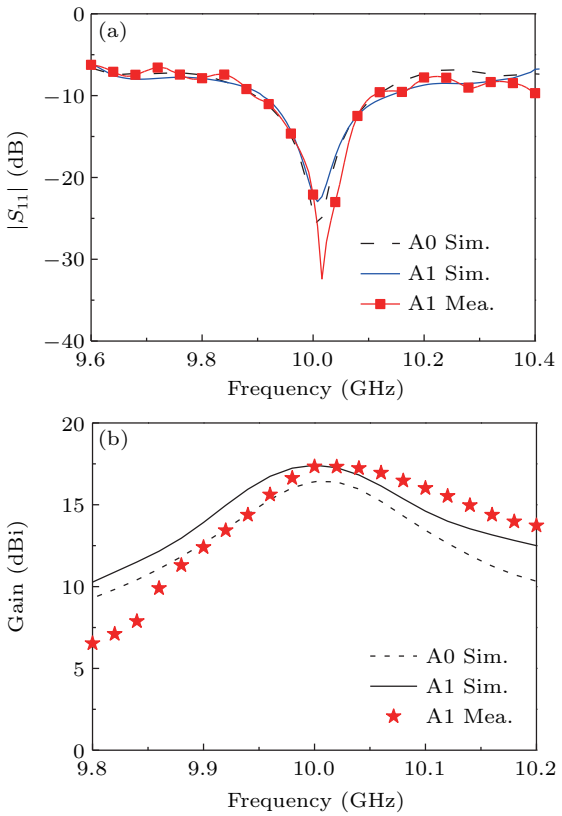


Fig. 11. Performance of antennas: (a) reflection coefficient, (b) gain.

A prototype of antenna 2 was fabricated and measured, and photographs are shown in Fig. 10. The experiment was conducted in an anechoic chamber. A vector network analyzer was used to measure the reflection coefficients of the antenna. The reflection coefficients of the antennas are shown

in Fig. 11(a). Antennas 1 and 2 have almost the same bandwidth. The measured −10 dB impedance bandwidth of antenna 2 is 9.9–10.1 GHz. Figure 11(b) plots the gains of the antennas. Compared with antenna 1, the gain of antenna 2 is improved throughout the operating bandwidth. The simulated maximum gains of two antennas at 10 GHz are about 16.5 dBi and 17.4 dBi, respectively, and the measured maximum gain of antenna 2 is 17.3 dBi, just 0.1 dBi lower than the simulated result. After optimization by the GA, the aperture efficiency of antenna 2 reaches to 94.5%.

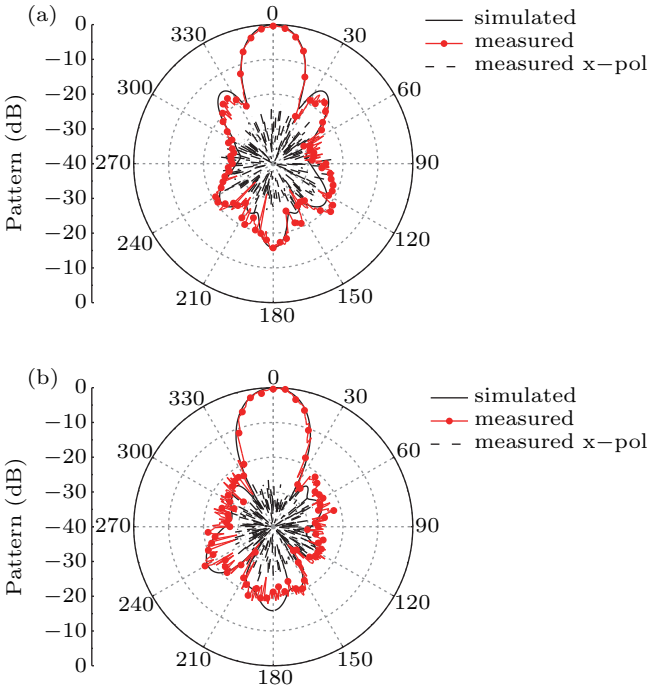


Fig. 12. Simulated and measured radiation patterns of the antenna in (a) the *xoz* plane and (b) the *yoz* plane.

Table 2. Comparison of the proposed antenna with previously reported antennas.

Ref.	Frequency (GHz)	Size	Max. gain (dBi)	Profile (λ_0)	Aperture efficiency
[7]	10.18	$1.36\lambda_0^2$	16.35	0.578	70.58%
[10]	11.4	$3.8\lambda_0^2$	15.75	0.6	77%
[12]	13.09	$11.33\lambda_0^2$	20.6	2.27	80.6%
[13]	5.8	$9.6\lambda_0^2$	19.4	1.04	91.7%
[14]	10	$12.9\lambda_0^2$	19.7	0.53	82.5%
Antenna 2	10	$4.5\lambda_0^2$	17.3	0.33	94.5%

Figure 12 plots the radiation patterns of the antennas in the *xoz* plane and *yoz* plane at 10 GHz. The measured results agree well with the simulated results in both planes. The side lobe levels of antenna 2 are lower than −16 dB, and the measured cross-polarization levels are less than −25 dB. The antenna has good radiation properties in the far field. Table 2 lists a comparison between the proposed antenna with and those in previous reported works. Compared with other antennas, the proposed antenna shows great progress in aperture efficiency, which reaches 94.5%. The proposed coupled receiver–transmitter MS gives the antenna a very high aperture efficiency with a simple structure.

5. Conclusion

A novel coupled receiver–transmitter MS is proposed in this paper. The antenna has a coupled receiver–transmitter MS as the PRS of the resonator cavity. The unit cell of the MS realizes wave transmission from the receiver patch to the radiator patch by means of slot coupling, which allows the characteristics of the antenna to be independently controlled. The MS is used as the PRS of the FP resonator antenna to realize high aperture efficiency of the antenna. The transmission coefficients of different unit cells on the MS were optimized by a GA. The antenna then presents nearly uniform electric amplitude and phase distribution across the aperture field and obtains gain enhancement in the far field. Finally, the improved antenna realizes a maximum gain of 17.3 dBi at 10 GHz. The aperture efficiency of the antenna is calculated to reach 94.5%. Compared with other high-gain resonator antennas, the proposed antenna obtains very high aperture efficiency with a low profile and simple structure.

References

[1] Liu G, Wang H J, Jiang J S, Xue F and Yi M 2015 *IEEE Anten. Wirel. Propag. Lett.* **14** 1415
[2] Tao Z, Jiang W X, Ma H F and Cui T J 2018 *IEEE Trans. Anten. Propag.* **66** 16
[3] Ren J Y, Jiang W, Zhang K Z and Gong S X 2018 *IEEE Anten. Wirel. Propag. Lett.* **17** 853
[4] Zarbakhsh S, Akbari M, Samadi F and Sebak A R 2019 *IEEE Trans. Anten. Propag.* **67** 16
[5] Trentini G V 1956 *IEEE Trans. Anten. Propag.* **4** 666
[6] Leger L, Serier C, Chantalat R, Thevenot M, Monediere T and Jecko B 2004 *Annal. Télécommun.* **59** 242
[7] Singh A K, Abegaonkar M P and Koul S K 2017 *IEEE Anten. Wirel. Propag. Lett.* **16** 2388
[8] Vettikalladi H, Lafond O and Himdi M 2009 *IEEE Anten. Wirel. Propag. Lett.* **8** 1422
[9] Dutta K, Guha D and Kumar C 2017 *IEEE Trans. Anten. Propag.* **65** 1399
[10] Lalbakhsh A, Afzal M U, Esselle K P, Smith S L and Zeb B A 2019 *IEEE Trans. Anten. Propag.* **67** 1916
[11] Afzal M U, Esselle K P and Zeb B A 2015 *IEEE Trans. Anten. Propag.* **63** 3390
[12] Lalbakhsh A, Afzal M U, Esselle K P and Smith S L 2019 *IEEE Trans. Anten. Propag.* **67** 1975
[13] Zhou L, Chen X and Duan X 2018 *IEEE Trans. Anten. Propag.* **66** 2061
[14] Xie P, Wang G M, Li H P, Liang J G and Gao X J 2019 *IEEE Access* **7** 176170
[15] Li H P, Wang G M, Cai T, Hou H S and Guo W L 2019 *Phys. Rev. Applied* **11** 014043
[16] Ji W Y, Cai T, Wang G M, Li H P, Wang C Y, Hou H S and Zhang C B 2019 *Opt. Express* **27** 2844